A Comparison Between Finite Element and Analytical Solutions of Interfacial Stress Distribution in a RC Beam Retrofitted with FRP Composites

Mohamad Zaman Kabir[i]; Ata Hojatkashani[ii]

ABSTRACT

The use of composite materials for strengthening of concrete structures has become a common practice in structural rehabilitation industry since last decade. The present study investigates the interfacial stresses between FRP fabrics and the concrete substrate in reinforced concrete (RC) beams. The methodology is based on an analytical manipulation which completes the previous investigations done by other researchers. Primarily, a closed form solution is developed to express the distribution of interfacial stresses along the bond length at the end of FRP plate where the concrete has linear behavior. In post-linear region, the analysis is performed at the cracked zone. In order to verify the analytical predictions, a numerical solution using FEM is performed. The main distinction between the work done in this paper and other researches, is examining the effect of the tensile steel reinforcement in concrete. This effect is analyzed at the plate end and at the cracked zone with linear and nonlinear behavior of concrete, respectively. Moreover, a parametric study is performed which considers the effect of the variety of adhesive thicknesses on the interfacial stresses between the concrete substrate and the FRP layer.

KEYWORDS

FRP fabrics, Rehabilitation, Crack, Interfacial Stresses, Reinforced Concrete, Post-linear Region.

1. INTRODUCTION

Over the past decade, the use of fiber reinforced plastics has been so popular among engineers. These materials were first introduced to the Mechanics and Aerospace Engineering applications. At the present, retrofitting of structures using FRP Materials is a common practice; and the application of them is a feasible way of increasing the load carrying capacity of structures.

Nowadays, structural rehabilitation obliges civil engineers to perform studies and research activities on the behavior of the FRP bars and sheets. Several modes of failure have been discussed by the researchers such as: FRP rupture, concrete crushing, compressive failure, and debonding. These failure modes are discussed in details in [1].

The debonding failure mode which occurs between FRP sheet and concrete surface is a common structural failure mode. Thus, recently the bond behavior has widely been discussed and analyzed by the researchers. References [2] and [3] presented stress contour plots of the FRP-anchorage zone based on the linear FE analysis. Several researchers such as [4] and [5] concluded that when beams with bonded plates are loaded in flexure, the failure mode is associated with delamination of the plate from the beam. References [6] and [7] developed analytical solutions for the shear and normal stresses along the interface between the bonded plate and the concrete beam.

Some researchers presented analytical models to investigate the interfacial stresses between bonded plate and the surface of the concrete beam at the FRP plate end. Reference [8] performed linear analytical models and compared them with other solutions. In a similar work, some parametric solutions were made and compared to the FE solution [9].

Although the interfacial stresses at the plate end play a significant role in the debonding failure mode of the FRP retrofitted concrete beams, the interfacial stresses at the cracked zone are more critical. In concrete beams, flexural and shear cracks are commonly found on the tensile side of the beam. Under loading, these cracks tend to open and induce high interfacial shear stresses. A recent work has made a fracture mechanics based analysis to obtain the

i M. Z. Kabir is with the Department of Civil Engineering, Amirkabir University of Technology, Tehran, Iran (e-mail: mzkabir@aut.ac.ir).

ii A. Hojatkashani is the Ph.D. Student in the Department of Civil Engineering, Amirkabir University of Technology, Tehran, Iran (e-mail: ata_hojat@aut.ac.ir).

crack mouth opening and the maximum interfacial shear stress at the cracked region for a given applied moment [10].

2. Objective of the Current Study

The main purpose of the present paper is to examine the effect of tensile steel reinforcement on the interfacial stresses in post-linear stage of concrete beam. First, a closed form solution is developed to express the distribution of normal and shear stresses at the plate end region. At this region, the concrete has linear characteristics. At the other stage, a solution is applied for calculation of tensile force in FRP fabric as a boundary condition to predict the shear stress function at the cracked zone where the concrete has nonlinear behavior. This method performs equilibrium equations based on strain compatibility condition. Finally, in order to verify the mathematical results, numerical finite element solution is presented.

3. Interfacial Stresses at the Plate End

To examine the effect of the tensile steel reinforcement at the linear stage, the section including concrete and steel is separated from the FRP plate. In order to consider the steel reinforcement in the equations, the reinforced concrete section is transformed in to concrete. Thus, in the equations the cross section area of steel would be assumed as $(n-1)A_s$. Consequently, the transformed moment of inertia and area of the section including concrete and the tensile steel reinforcement , I_{trc} and A_{trc} , are calculated as:

$$I_{trc} = \frac{w_c h^3}{12} + w_c h\left(\frac{h}{2} - c\right)^2 + (n-1)A_S(d_S - c)^2 \quad (1)$$

$$A_{trc} = A_c + (n-1)A_S = w_c h + (n-1)A_S$$

Figure 1 shows the loading condition and the beam section. The following assumptions are used in the analytical model:

1. At the plate end, the concrete behaves linearly. However, at the cracked zone, the material has nonlinear characteristics as described in section 4.
2. The adhesive and FRP materials behave elastically and linearly.
3. No slip is allowed at the interface of the bond.
4. Since it is assumed that both the adhesive and FRP plate are very thin, stresses in the adhesive layer and composite materials do not change with thickness.
5. The bending stiffness of the concrete beam is much greater than the stiffness of the FRP plate.

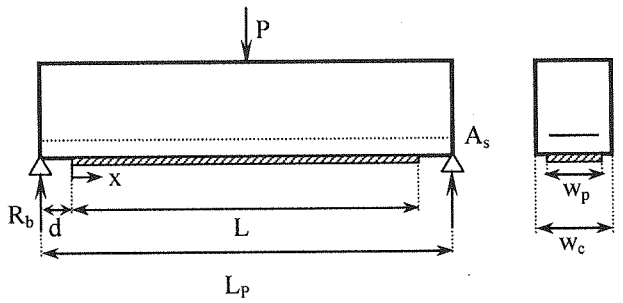

Figure 1: Loading condition and section.

A. Interfacial Shear Stress

Considering $\varepsilon_P(x)$ and $\varepsilon_C(x)$ as strains in FRP and concrete layer, respectively. the differentiation of the shear stress with respect to x, is:

$$\frac{d\tau(x)}{dx} = \frac{G_a}{t_a}\left(\varepsilon_p(x) - \varepsilon_c(x)\right) \quad (2)$$

where G_a and t_a are the shear modulus and the thickness of the adhesive layer, respectively. By using a simplification, the strain relation for the plate would be [9]:

$$\varepsilon_p(x) = \frac{N(x)}{E_p t_p w_p} \quad (3)$$

where E_P is the FRP effective modulus of elasticity, t_P and w_P are the FRP plate thickness and width respectively. Also, the strain in concrete is:

$$\varepsilon_c(x) = \frac{M_c(x)y_c}{E_c I_{trc}} - \frac{N(x)}{E_c A_{trc}} \quad (4)$$

The above equation is taken from [8]. In this research the effect of the tensile steel bar is introduced by using I_{trc} and A_{trc}. $M_C(x)$ is the applied moment on the concrete layer, N(x) is the axial force acting on concrete or FRP layer, E_C and y_C are concrete modulus of elasticity and distance from the bottom of the reinforced concrete section to its centroid, respectively.

The equation below [8], explains the relation between the total moment in the section and the moment applied in the concrete layer M_c (x), and the moment applied in the FRP layer M_p (x):

$$M_T(x) = M_c(x) + M_p(x) + N(x)(y_c + y_p + t_a) \quad (5)$$

$$M_c(x) = RM_p(x) \quad , \quad R = \frac{E_c I_{trc}}{E_p I_p}$$

y_p is the distance from the top of the FRP layer to its centroid and I_P is the moment of inertia for FRP plate. In Figure 2 for the description of y_c , y_p and t_a , a schematic pattern of the layers is illustrated.

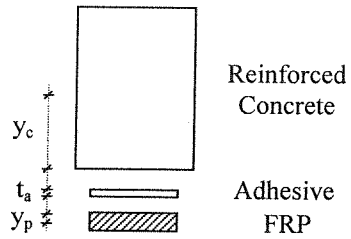

Figure 2: Different layers of a retrofitted RC beam.

By substitution of (3) to (5) into (3) and solving the resulted differential equation with its boundary conditions as indicated in [9], the shear stress relation becomes

$$\tau(x) = C_1\cosh(\beta x) + C_2\sinh(\beta x) + \eta_0 \qquad (6)$$

where:

$$C_1 = -C_2 = \frac{G_a y_c R_b . d}{t_a E_c I_{trc} \beta}\ ,\quad \eta_\circ = \frac{R\, G_a\, y_c\, R_b}{(R+1) E_c\, I_{trc}\, t_a \beta^2},$$

$$\beta = \left\{\frac{G_a}{t_a}\left[\frac{1}{E_p t_p} + \frac{R}{R+1}\cdot\frac{y_c}{E_c I_{trc}}.w_p\left(y_c + y_p + t_a\right) + \frac{w_p}{E_c A_{trc}}\right]\right\}^{0.5} \qquad (7)$$

B. Interfacial Normal Stress

The following equation expresses the interfacial normal stress [8]:

$$\sigma(x) = \frac{E_a}{t_a}\left[v_p(x) - v_c(x)\right] \qquad (8)$$

where $v_p(x)$ and $v_c(x)$ are the vertical displacements in the FRP and concrete layer, respectively.

Plugging the following elastic moment-curvature relations into (8):

$$\frac{d^2 v_c(x)}{dx^2} = -\frac{1}{E_c I_{trc}} M_c(x)\ ,\quad \frac{d^2 v_p(x)}{dx^2} = -\frac{1}{E_p I_p} M_p(x) \qquad (9)$$

a differential equation is obtained, where its solution turns out the following expression for normal stress as:

$$\sigma(x) = e^{-\lambda x}\left[H_1 \mathrm{Cos}(\lambda x) + H_2 \mathrm{Sin}(\lambda x)\right] - n_1 \frac{d\tau}{dx} \qquad (10)$$

in which:

$$\lambda = \left\{\frac{E_a}{4 t_a} w_p\left[\frac{1}{E_p I_p} + \frac{1}{E_c I_{trc}}\right]\right\}^{0.25},$$

$$n_1 = \frac{1}{4\lambda^4 + \beta^4}\cdot\frac{E_a}{t_a} w_p\left[\frac{y_c}{E_c I_{trc}} - \frac{y_p}{E_p I_p}\right] \qquad (11)$$

H_1 , H_2 are constants which can be defined by applying the boundary conditions as exactly explained in [8].

4. Interfacial Shear Stress at the Cracked Location at Midspan of Beam Using Strain Compatibility Condition

Using strain compatibility, the equilibrium equations are performed at the cracked section of the beam. At this section, the concrete portion behaves nonlinearly and the tensile part is neglected. The equilibrium equations at the cracked section are;see Figure 3:

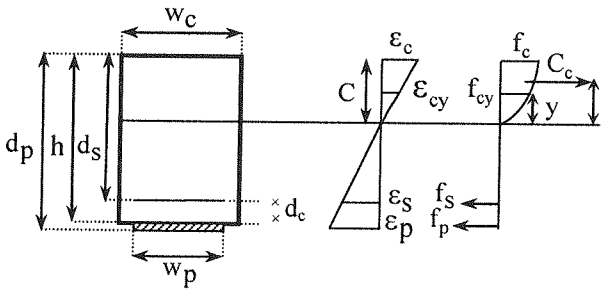

Figure 3: Geometry of the section and strain .

$$\begin{cases} C_c - f_s A_s - f_p A_p = 0 \\ C_c \times \bar{y} + A_s f_s (d_s - c) + A_p f_p (d_p - c) = M_T(x) \end{cases} \qquad (12)$$

where C_c and $\bar{y}$, are the overall compression force in the concrete under pressure and its distance from the neutral axis, respectively. The mentioned equilibrium equations will help to find out the FRP tensile force at the cracked region, as designated N_P. Calculation of N_P via the equilibrium equations (12) would result in a boundary condition which helps to find the shear stress relation. In order to obtain the shear stress relation at the cracked region, x variable should be transformed into $\frac{L}{2} - x$ in (6) as the following:

$$\tau(x) = C_1 \mathrm{Cos\,h}\left[\beta\left(\frac{L}{2} - x\right)\right] + C_2 \sin h\left[\beta\left(\frac{L}{2} - x\right)\right] + \eta_\circ \qquad (13)$$

5. Finite Element Solution

For the validation of the analytical results, a finite element approach is, also, performed in this research. Ansys 9.0 FEM software is used to model the rectangular beam strengthened by an externally bonded FRP plate subjected to the three-point bending load. The three_ dimensional model used for the numerical analysis is illustrated in Figure 4. In order to have an appropriate verification, all the assumptions used in the analytical solution are implemented in the FE model. The selected numerical model used for concrete is 8node solid65 element with the capabilities of material nonlinearities. The interface adhesive and FRP are modeled using 8node solid45 element with linear characteristics. Also, for modeling of the tensile steel rebars, link8 element (3-D spar) is used.

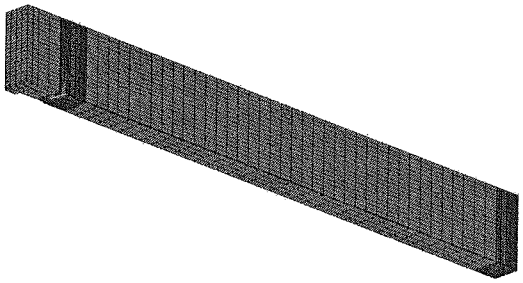

Figure 4: 3D numerical model.

A. Description on the Presented Model

Using the benefit of symmetry, only a quarter of the beam is modeled. The model is cut along the longitudinal and transverse axes of the beam. For examining the stress distribution, the mesh pattern is fined at the plate end and at the cracked locations.

One of the important issues in the numerical analysis of an externally strengthened structure, is the modeling of the adhesive layer. Owing to the fact that the main purpose of the research is examining the shear stress distribution in the adhesive layer at the early stages of loading, according to the formation of the primary crack pattern, no failure criterion is assigned for the material details of the adhesive. Moreover, the mechanical specifications of the adhesive itself are identical in all directions, i.e, it has an isotropic behavior.

Another important point in modeling of the adhesive is the number of layers which should be considered in the FE modeling of the adhesive. Since the adhesive should react between substrate surface and FRP, for the better compatibility between the two major parts, the adhesive is modeled by 3 layers. The thickness of the three layer adhesive is considered 0.1 mm. Figure 5 shows the numerical model of adhesive and FRP.

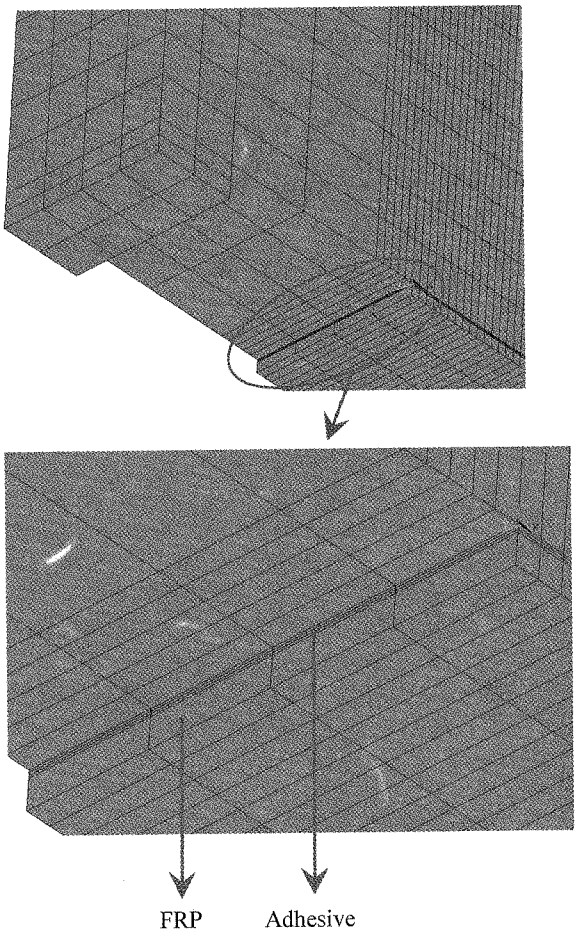

Figure 5: Adhesive and FRP.

Another important feature in the FE analysis is the crack pattern in the model. The crack pattern in the concrete elements is introduced as the smeared crack pattern. At the first steps of loading, the crack pattern in the concrete is illustrated as a single row of cracked elements. This pattern is defined here as the primary crack pattern. By increasing the load, the uniform single row crack pattern turns to multiple rows of cracked elements. This crack pattern is defined as secondary crack pattern.

Figure 5 shows the primary and secondary crack patterns in the unreinforced and reinforced concrete beam. The interfacial shear stresses are examined for the primary crack pattern. For the model when there is tensile steel with A_s=1000 mm^2 the stress distribution at the cracked region before and after the formation of the secondary cracks is presented in Figure 6. When there is primary crack pattern, there is an exponential stress diagram at the cracked region. But when secondary cracks form along the beam, there is an oscillatory crack pattern, and peak points of this pattern indicate maximum stress at the vicinity of the cracks, as illustrated in Figure 6.

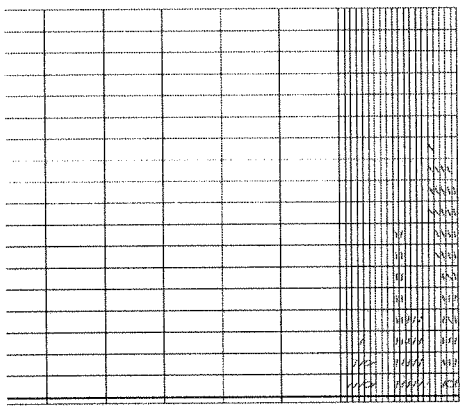

Figure 5-a: Primary cracks pattern in the unreinforced beam.

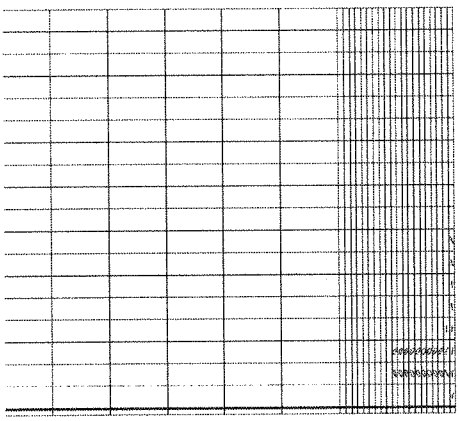

Figure 5-b: Primary cracks pattern in the reinforced beam.

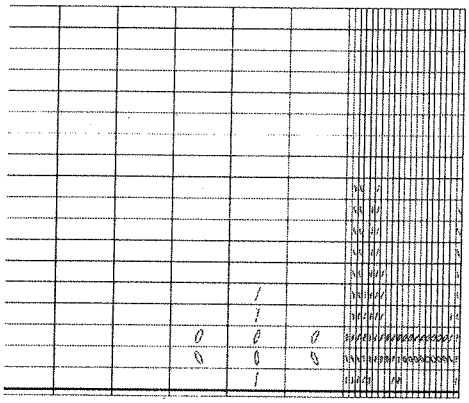

Fig`ure 5-c: Secondary cracks pattern in the reinforced beam.

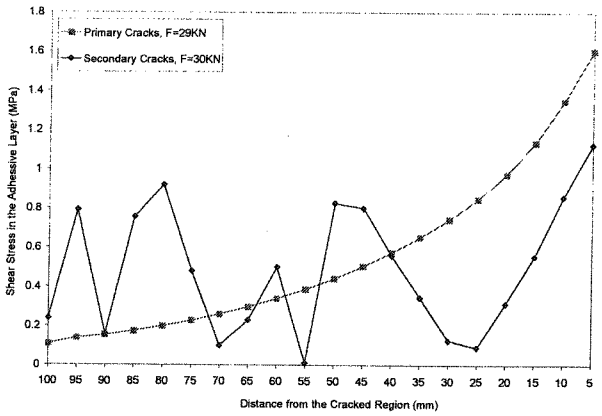

Figure 6: Interfacial stress distribution before and after the formation of the secondary cracks, A_s=1000 mm^2.

6. Results Verification

Based on the analytical and FE solutions, some verifications are presented in this section. The model is a simply supported beam with a point load acting at the midspan as previously illustrated in Figure 1.

It has to be mentioned that in all the proceeding results, the following assumptions are considered:

-The tensile steel yielding stress is assumed as f_y=280MPa

-According to [11], the relation between the modulus of elasticity and the compressive strength of concrete would be expressed as:

$$E_C = 4.7794\sqrt{f'_C} \qquad (14)$$

where E_C is in GPa and f'_C is in MPa.

-The tensile stresses in FRP and steel are calculated as the following linear relations:

$$f_p = E_p\varepsilon_p \ , \ f_s = E_s\varepsilon_s \qquad (15)$$

-The assumption for the concrete cover is d_c=50mm , from which the length d_s can be simply obtained.

For the first part of this section, verification with an experimental result according to [9] is presented. This verification is depicted In Figure 7 where the effect of tensile steel reinforcement on the strain in FRP at the plate end is examined. The geometry and material specifications used in Figure 7 are: L_P=400mm, L=350mm, h=w_p=w_c=150mm, t_a=0.1mm, t_P=1.6mm, E_a=3.3GPa, ν_a=0.435, E_P=159GPa, E_c=27.8GPa, E_s=200GPa.

In this part of the specimen, where concrete has linear behavior, the relation between the applied force and the axial strain in FRP layer is depicted. Based on the experimental and the finite element solution adopted from [9] and the solution presented, it can be seen that a good correlation between experimental, FE and current study exists. Figure 7 also, shows that for a specific applied force, as the tensile steel increases, the strain in FRP reduces.

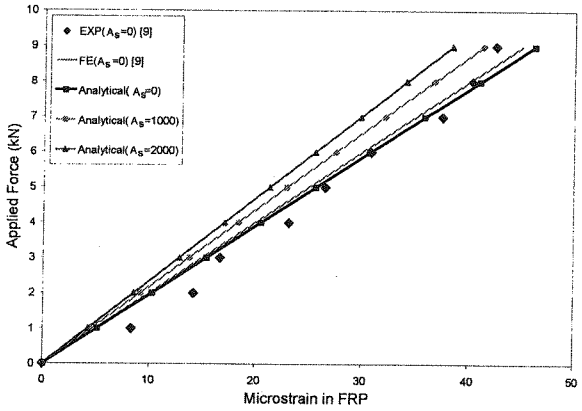

Figure 7: Comparison between the experimental, FE and analytical solutions, A_s is in mm^2.

For the rest of the results, some simulations are given to examine and compare FE with analytical solutions. In this respect and in order to illustrate evident stress distributions, an alternative model is presented. The geometry and the material specifications are changed. Thus, in Figures 8 to 20, the geometry of the beam and the materials specifications are: L_P=4500mm, L=4200mm, h=450mm, w_p=w_c=200mm, t_a=1.5mm, t_P=6mm, E_a=0.814GPa, ν_a=0.37, E_P=37.23GPa, , E_c=27.99GPa, E_s=200GPa.

In Figures 8 and 9, the concrete beam is simply supported under central point load with the amount of P=100kN. The effect of the tensile steel reinforcement on the interfacial stresses at the plate end is illustrated in the figures. It can be observed that as the reinforcement increases, the interfacial stresses reduces. It is also shown that the critical zone at the FRP plate end for the shear stress distribution, is much grater than the one for the normal (peeling off) stress distribution. The critical length for the shear stress distribution is about 140mm. This length for the normal stress distribution, where the stress is tensile, is about 10mm.

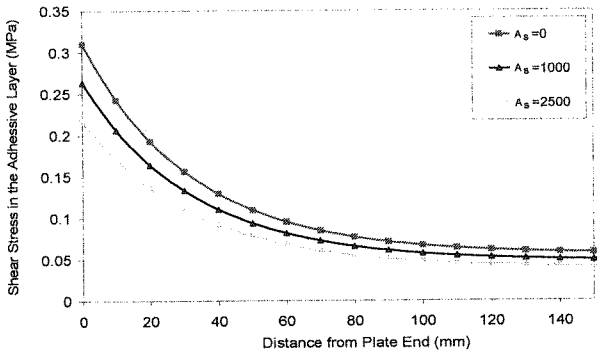

Figure 8: The effect of the tensilesteel bars on the interfacial shear stress at the end plate based on the analytical solution, A_s is in mm^2.

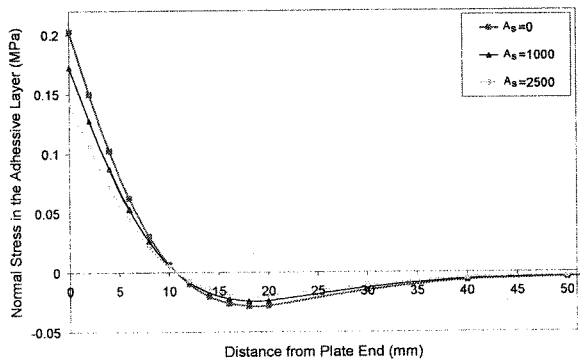

Figure 9: The effect of the tensional steel bars on the interfacial normal stress at the end plate based on the analytical solution, A_s is in mm^2.

Table 1 shows the corresponding applied loads induced primary and secondary cracks, calculated both in analytical and numerical solutions. The difference between the analytical and the numerical results indicates that the mathematical solution gives overestimation of applied load prior to the first crack and the numerical solution considers more flexibilities of the beam behavior.

The effect of the tensile reinforcement on the interfacial shear stresses at the cracked region in midspan is presented in Figure 10. Application of a point load of about 28.5kN results in the formation of the primary crack pattern. From this figure, it can be seen that increasing the tensile steel reinforcement reduces the interfacial stresses. The interfacial shear stress decays in a parabolic manner with the maximum amount at the neighborhood at cracks position towards a distance apart from the cracks position about 100 mm and it could be negligible.

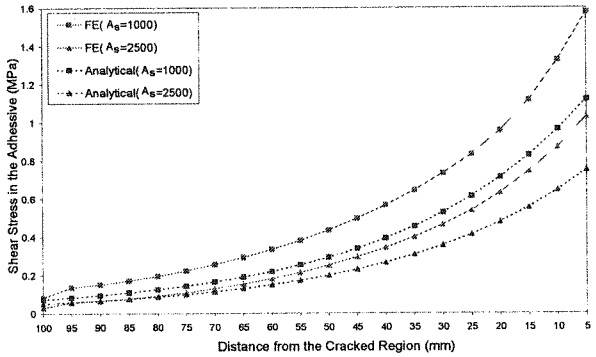

Figure 10: The effect of the tensional steel reinforcement on the interfacial shear stress at the cracked region. Comparison between the analytical and FE solutions. A_s is in mm^2.

TABLE 1. PRIMARY AND SECONDARY CRACKS LOADS BASED ON THE ANALYTICAL AND NUMERICAL RESULTS

	Analytical method (equilibrium equations in the section)	Numerical method	
	Primary cracks load	Primary cracks load	Secondary cracks load
Unreinforced beam	23.5 kN	19.25 kN	-
A_S=1000 mm^2(4Φ18)	27.5 kN	22.25 kN	29 kN
A_S=2500 mm^2(4Φ28)	34 kN	27.25 kN	37.75 kN

The interfacial shear and normal stresses obtained from the analytical and the FE solutions for the situation of unreinforcement, are sketched versus distance from FRP plate end in Figure 11. A central point load of 25kN is applied under which the cracking of the beam starts according to the analytical solution. It can be observed that the critical length in the FRP plate end in which the interfacial stresses are active is about 20mm for shear stress and 12mm for normal stresses. The latter one is tensional at the vicinity of end plate up to 3mm and its compressive between 3mm to 12mm from FRP plate end.

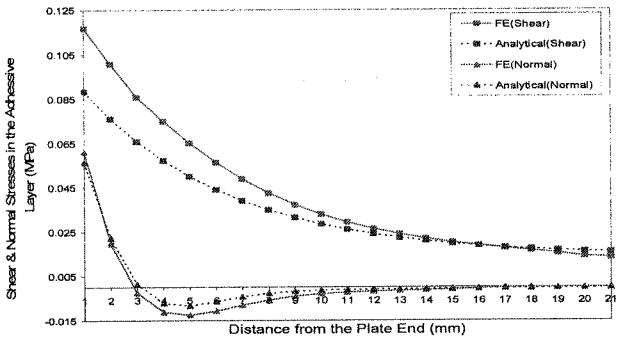

Figure 11: Comparison between the analytical and FE solutions for the interfacial stress at the plate end for the unreinforced beam.

In Figures 12 and 13, when a mid-span point load of P=29kN,which is the load prior to the formation of the secondary cracks, is applied to the beam with the reinforcement of A_s=1000 mm^2, the variation of interfacial stresses are presented at the critical distance from cracked region and FRP plate end. In these figures, the results from the FE and the analytical solutions are compared. By comparing these figures, it can be concluded that the interfacial stresses at the cracked zone are much higher than those at the plate end. Also, it can be seen that the critical length in the FRP plate at the plate end and the cracked zone in which there is the shear stress distribution, are almost identical and are about 100mm from the plate end and from the cracked location respectively. The critical length for the normal stress distribution at the plate end is about 10mm which is much smaller than the one for the shear stress distribution.

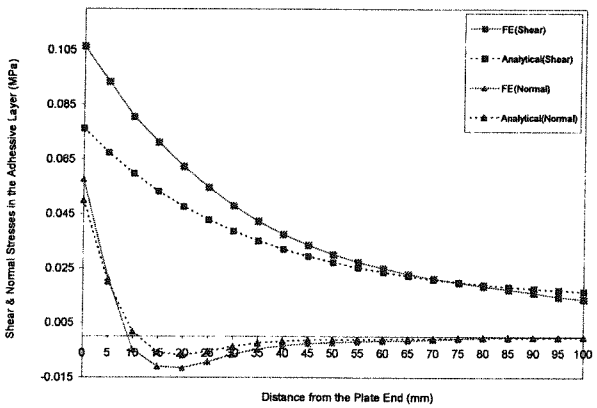

Figure 12: Comparison between the analytical and FE solutions for the interfacial stress at the plate end, A_s=1000 mm^2.

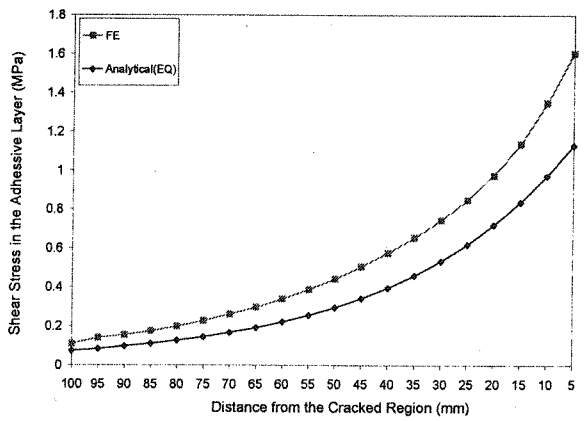

Figure 13: Comparison between the analytical and FE solutions for the shear stress at the cracked region, A_s=1000 mm^2.

In Figures 14 and 15, a point load of P=37.25kN which if the load prior to the formation of secondary cracks, is applied to the beam with the reinforcement of A_s=2500mm^2. The interfacial stresses at the plate and at the cracked zone are examined. In these Figures, FE and analytical solutions are compared. Again, by comparing these figures it can be concluded that the interfacial stresses at the cracked zone are much higher than those at the plate end. Similar to the previous results, it can be observed that the critical length in the FRP plate at the plate end and the cracked zone in which there is the shear stress distribution, are about 100 mm from the plate end and from the cracked location, respectively. In addition, the critical length for the normal stress distribution at the plate end is about 10mm.

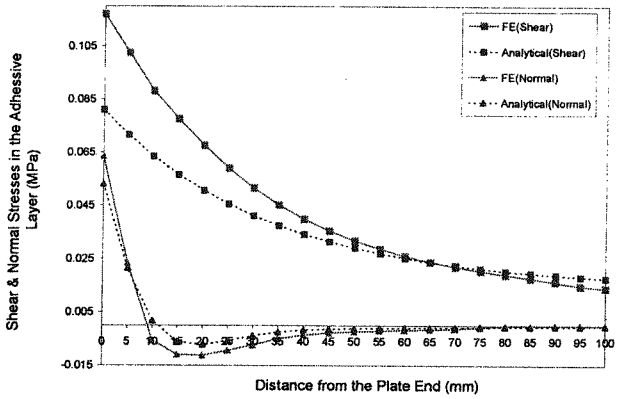

Figure 14: Comparison between the analytical and FE solutions for the interfacial stress at the plate end, A_s=2500 mm^2.

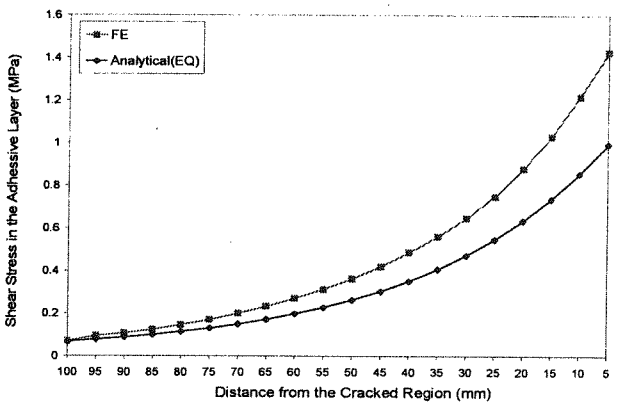

Figure 15: Comparison between the analytical and FE solutions for the shear stress at the cracked region, A_s=2500 mm^2.

Finally, in Figures 16 to 20 a parametric study on the variety of the thickness of the adhesive is presented. In these results, the beam has tensile steel reinforcement ,A_s=1000 mm^2 , and a point load of P=24.25kN is applied to the beam. This is the load under which the cracking condition from FE and analytical solutions would be almost similar. In these Figures, analytical and FE solutions are compared. Figure 16 shows the effect of the thickness of the adhesive on the interfacial shear stress at the cracked zone. In Figures 17 to 20, the effect of the thickness of the adhesive on the interfacial stresses at the plate, are examined.

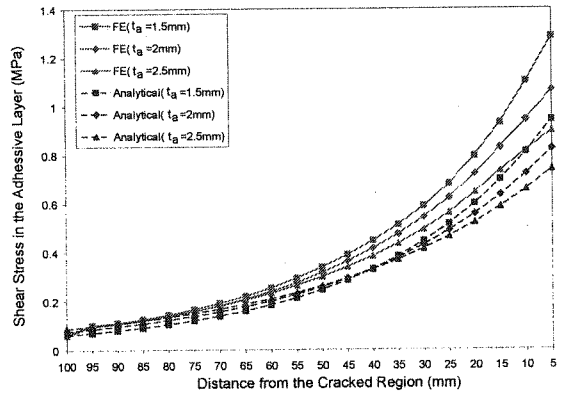

Figure 16: The effect of the variety of thickness of the adhesive on shear stress at the cracked region based on the results obtained from the analytical and the FE solutions, A_s=1000mm^2.

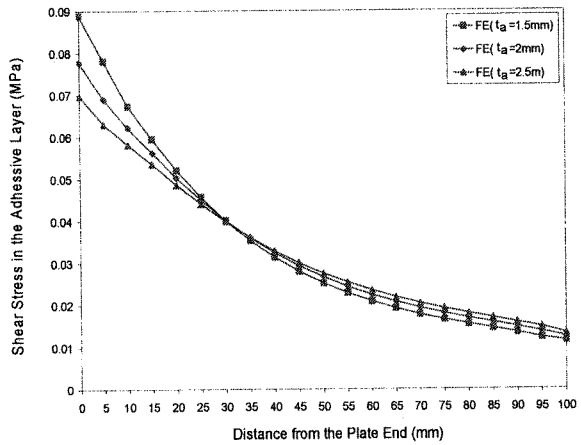

Figure 17: The effect of the variety of thickness of the adhesive on shear stress at the plate end based on the results obtained from the analytical solution, A_s=1000 mm^2.

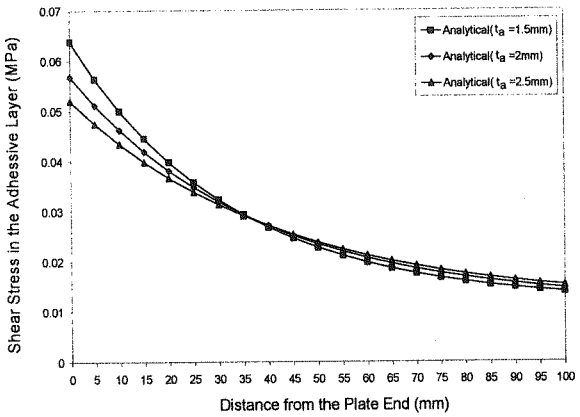

Figure 18: The effect of the variety of thickness of the adhesive on shear stress at the plate end based on the results obtained from the analytical solution, A_s=1000 mm^2.

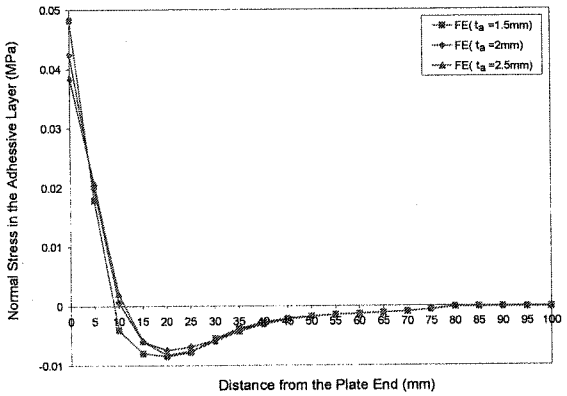

Figure 19: The effect of the variety of thickness of the adhesive on normal stress at the plate end based on the results obtained from the FE solution, A_s=1000 mm^2.

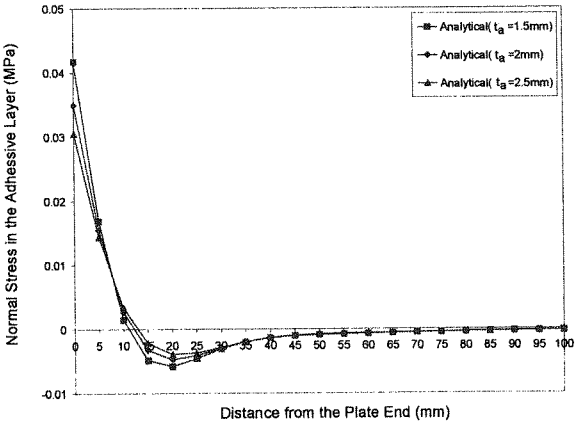

Figure 20: The effect of the variety of thickness of the adhesive on normal stress at the plate end based on the results obtained from the FE solution, A_s=1000 mm^2.

Similar to the previous results, it can be observed that the critical lengths in the FRP plate at the plate end where there is the shear and the normal stress distribution, are about 100mm from the plate end for the shear stress and 10-12mm for the normal stress distribution.

From all the simulations in the parametric study section, it can be concluded that by increasing the thickness of the adhesive layer the interfacial stresses decrease.

7. CONCLUSIONS

Based on the current research, the interfacial stresses in a retrofitted RC beam are seen to be critical at two locations. One at the plate end and the other at the cracked zone. Analytical and FE solutions are presented to predict these stresses at the plate end and at the cracked section when there is one single crack at the middle section of the beam. In order to define the stress distribution at the cracked region, the equilibrium method using strain compatibility condition is implemented. For the beams with tensile steel reinforcement, the analytical and FE solutions are compared with each other. The intensive parametric studies are carried out to examine the influence

of tensile steel reinforcement and adhesive thickness on the interfacial stress distribution. Based on the results obtained from the analytical and the FE solutions when the tensile steel increases, the interfacial stresses are declined. The thickness of the adhesive has a similar effect, that is, when the thickness of the adhesive increases the interfacial stresses decrease.

Based on the FE results, before the formation of the secondary cracks, the stress distribution pattern at the cracked region is continuum and exponential. But after the formation of the secondary cracks, this stress pattern becomes non-uniform and noisy specifically at the cracked locations. Therefore, here, assuming the nonlinear characteristics of the concrete, the results would be closer to the experimental ones.

Finally, comparing the analytical and the FE results, there would be observed a difference of about 10-20%. The difference rises by increasing the cross section of the reinforcement used. This would be because of the difference of the condition of the application of the tensile steel in the analytical and the FE solutions. There is no doubt that the FE solutions considers more flexibility and degrees of freedom in the model and hence, gives more precise results. However, a closed form solution with some approximations recommended in this research, would be obviously a less time consuming and proper effort for estimation and prediction of the interfacial stress distribution in a RC beam retrofitted with FRP.

8. REFERENCES

[1] J.G. Teng, and J.F. Chen, and S.T. Smith, *FRP-Strengthening RC Structures*, New York, NY, USA, John Wiley & Sons, LTD, 2002.

[2] J.G. Teng, and J.W. Zhang, and S.T. Smith, "Interfacial Stresses in Reinforced Concrete Beams Bonded with a Soffit Plate: A Finite Element Study," *Construct Build Mater*, vol. 16, pp. 1-14, 2002.

[3] N. Pesic, and K. Pilakoutas, "Concrete Beams with Externally Bonded Flexural FRP-Reinforcement: Analytical Investigation of Debonding Failure," *Journal of Composites, PartB: Engineering*, vol. 34, pp. 327-338, 2002.

[4] H. Saadatmanesh, and M.R. Ehsani, "RC Beams Strengthened with FRP Plates, I: Experimental Study," *Journal of Structural Engineering, ASCE*, vol. 117, pp. 3417-3433, 1991.

[5] U. Meier and M. Deuring and H. Meier and G. Schwegler, "Strengthening of Structures with CFRP Laminates," in *Proc. 1992 CSCE Research and Applications in Switzerland. Advanced Composite Materials in Bridges and Structures*, pp..243-251.

[6] B. Taljsten, "Strengthening of Beams by Plate Bonding," *J. Mat. In Civ. Engrg., ASCE*, vol. 9, pp. 206- 212, 1997.

[7] A.M. Malik, and H. Saadatmanesh, and M.R. Ehsani, "Prediction of Failure Load of R/C Beams Strengthened with FRP Plate due to Stress Concentration at the Plate End," *ACI Struct. J.*, vol. 95, pp. 142-152, 1998.

[8] S.T. Smith, and J.G. Teng, "Interfacial Stresses in Plated Beams," *Journal of Engineering Structures*, vol. 23, pp. 857-871, 2001.

[9] K.T. Lau, and P.K. Dutta, and L.M. Zhou, and D. Hui, "Mechanics of Bonds in an FRP Bonded Concrete Beam," *Journal of Composites, PartB: Engineering*, vol. 32, pp. 491-502, 2001.

[10] C.K.Y. Leung, "Delamination Failure in Concrete Beams Retrofitted with a Bonded Plate," *Journal of Materials in Civil Engineering, ASCE*, vol. 13, pp. 106-113, 2001.

[11] Building Code Requirements for Structural Concrete (ACI 318-05) and Commentary (ACI 318R-05), 2005.